http://dx.doi.org/10.5935/0103-5053.20150066

J. Braz. Chem. Soc., Vol. 26, No. 5, 1004-1012, 2015.
Printed in Brazil - ©2015 Sociedade Brasileira de Química
0103 - 5053 $6.00+0.00

Article

Silver Nanoparticle Thin Films Deposited on Glass Surface Using an Ionic Silsesquioxane as Stabilizer and as Crosslinking Agent

Andressa C. Schneid,[a] Marcelo B. Pereira,[b] Flavio Horowitz,[b] Raquel S. Mauler,[a] Carla R. Matte,[c] Manuela P. Klein,[c] Plinho F. Hertz,[c] Tania M. H. Costa,[a] Eliana W. de Menezes,[a] and Edilson V. Benvenutti*,[a]*

[a]*Instituto de Química, UFRGS, CP 15003, 91501-970 Porto Alegre-RS, Brazil*

[b]*Instituto de Física, UFRGS, CP15015, 91501-970 Porto Alegre-RS, Brazil*

[c]*Instituto de Ciência e Tecnologia de Alimentos, UFRGS, CP 15095, 91501-970 Porto Alegre-RS, Brazil*

Thin films containing silver nanoparticles homogeneously dispersed, with narrow size distribution below 10 nm, were synthesized on flat glass surface, by using an ionic silsesquioxane as stabilizer and crosslinking agent. The films can be prepared without previous functionalization of substrate surfaces and without addition of other components. The films were heat treated up to 200 ºC and characterized by ultraviolet-visible, transmission electron microscopy, atomic force microscopy, thermogravimetric analysis and ellipsometry. The films were thermally stable when heated up to 200 ºC, presenting the same thickness, and maintaining both optical and morphological properties of silver nanoparticles. The antibacterial activity of the films, containing the silver nanoparticles, was evaluated against *Staphylococcus aureus* by using the film applicator coating method, showing an excellent performance even after the third cycle of sterilization.

Keywords: sol-gel hybrid materials, charged organosilane, thin films, antimicrobial activity

Introduction

In the last decade, thin films containing metal nanoparticles have been used as catalysts,[1-5] antimicrobial coatings[5-12] as well as optical,[1,13-15] electrochemical,[16-18] and photovoltaic devices.[19-21] These applications are possible due to the metal nanoparticles small size, which imparts unique properties such as absorption plasmon resonance band and high surface area.[22-24] Several forms for the preparation of metal nanoparticles films on solid substrates were already reported, such as, vapor-deposition methods,[8,25,26] sol-gel deposition of metal ions followed by thermal treatment[4-6,27-30] and also, the deposition of metal nanoparticles from colloidal dispersions.[10,14,31-34] The common substrate has been glass, but the poor adhesion of metal nanoparticles to glass frequently results in system instability under immersion or under thermal treatment,[33,35] characterized by morphological changes and particle coalescence. The thermal treatment, which is necessary to obtain or to fix the metal nanoparticles on the glass surfaces, can cause changes in the properties of the films.[27-31,35,36]

Each method has its own merits, but the colloidal deposition provides the possibility of using a diversity of nanoparticles sizes and shapes. In order to control the size and shape of the metal nanoparticles and overcome their thermodynamic instability, which leads to the formation of agglomerates, it is necessary the use of stabilizing agents.[24,37] The more common stabilizers are ionic liquids, soluble polymers, dendrimers and surfactants.[24,33,37-39] Although the stabilizers provide homogeneous liquid dispersion, which is essential for the film preparation, they do not contribute to the metal nanoparticles adhesion to the substrate surfaces. In this context, in most of the flat film preparation methods it is necessary the use of additional chemical procedures to promote the adhesion of the metal nanoparticles to the surfaces by crosslinking or previous surface functionalization, using linking agents such as silicon and titanium alkoxides[4-6,27-29] or organosilanes.[9,14,30-33,35] These agents form polymeric networks on the surfaces enabling the adhesion of nanoparticles.[27,28,31] However, some subjects deserve

*e-mail: eliana@iq.ufrgs.br, benvenutti@ufrgs.br

more studies, such as, the decrease in metal nanoparticles concentration on the surface, due to the barrier produced by the crosslinking agents and also by the interactions of the metal nanoparticles with the substrate, which is caused by the thermal treatment.[5,29,31,33] Additionally, the thermal treatment can promote the partial metal oxidation.[27-29] These effects produce morphological and chemical changes in the film properties.

Thin silver nanoparticle films are particularly important due to the inherent properties of silver, such as the good inhibitory and antimicrobial efficacy gainst a significant number of bacteria, viruses and yeasts, without producing microbial resistance.[40-44] Antimicrobial properties of silver in the form of ions, nanoparticles or composite nanodevices based on thin Ag films have been widely reported.[5-10] Besides the antibacterial properties, the biocompatibility and cytotoxicity of such materials have to be considered too.[45,46]

Recently, it was reported that ionic silsesquioxanes could be used as metal nanoparticle stabilizers.[47] These hybrid organic-inorganic materials have as organic moiety an ionic group such as quaternary ammonium group. Due to the presence of the ionic organic group, these materials exhibit appreciable solubility in water.[48,49] Therefore, in the same way of ionic liquids, they can be used as metal nanoparticle stabilizers.[47,50] However, compared to the ionic liquids, the metal nanoparticle/ionic silsesquioxane systems present advantages, since they can be evaporated, transformed into solid form, stored and completely re-dispersed in water, without any changes in the optical and morphological properties of the metal nanoparticles.[47] Therefore, these systems open the possibility to reusing them as a source of metal nanoparticles in the preparation of new materials.[47,50] Additionally, the ionic silsesquioxanes have also the inorganic silica component, which contains polymerizable silanol groups, allowing the possibility of obtaining hybrid materials with varied organic/inorganic content,[48,51,52] as well as, enabling to obtain covalently attached silsesquioxane films on silica or other inorganic matrix surfaces.[53-55] In a recent report, it was demonstrated that ionic silsesquioxane/silver nanoparticle system shows excellent antibacterial activity and low cytotoxicity, in aqueous medium.[56] The high antibacterial activity was interpreted considering the synergic effect of the ammonium quaternary groups and silver nanoparticles. Therefore, with these combined characteristics, the ionic silsesquioxanes became promising for the preparation of strongly adhered films that contain metal nanoparticles onto inorganic surfaces, to be applied as antibacterial coatings.

In this work, the ionic silsesquioxane containing the 1,4-diazoniabicyclo[2.2.2]octane nitrate group was prepared. This ionic silsesquioxane was used as stabilizer of silver nanoparticles in aqueous medium. The system metal nanoparticle/ionic silsesquioxane was employed for the first time to obtain thin films of silver nanoparticles onto flat glass surfaces. The films were heat-treated at several temperatures and they were characterized by ultraviolet-visible (UV-Vis) spectroscopy, transmission electron microscopy (TEM), atomic force microscopy (ATM), thermogravimetric analysis (TGA), spectral ellipsometry and antibacterial activity against *Staphylococcus aureus*.

Experimental

Chemicals

3-chloropropyltrimethoxysilane (CPTMS), 1,4-diazabicyclo [2.2.2]octane (DABCO) and *N*,*N*-dimethylformamide were purchased from Aldrich. Methanol and hydrofluoric acid were obtained from Merck. Formamide, silver nitrate and sodium borohydride were acquired from Vetec and sodium nitrate was purchased from Neon. Broth for bacteria growth was purchased from Merck. All chemicals employed were of analytical grade and used as received without any further purification.

Synthesis of ionic silsesquioxane

The ionic silsesquioxane that contains the double charge 1,4-diazoniabicyclo[2.2.2]octane nitrate group was synthesized according to previous reports.[57] Briefly, 5.605 g of DABCO (30 mmol) were dissolved in 40 mL of *N*,*N*-dimethylformamide, under argon atmosphere. After that, 11.4 mL of CPTMS (60 mmol) were added. The mixture was heated at 75 °C, upon stirring for 72 h, under inert atmosphere, until a white solid was formed. Then, the formed solid product was washed with methanol and dried for 2 h at 70 °C, and after that, the white solid was dissolved in 40 mL of formamide, under constant stirring at 70 °C, and 0.8 mL of water with five drops of hydrofluoric acid were added. The mixture was stored for gelation and evaporation of solvent at 40 °C, to obtain the ionic 1,4-diazoniabicyclo[2.2.2]octane chloride silsesquioxane. In order to obtain the ionic silsesquioxane with nitrate as counter ion, it was performed an ion exchange process, where chloride was replaced by nitrate. The ion exchange process was carried out using cold $NaNO_3$ 1 mol L^{-1} solution and it was evaluated by chloride potentiometric analysis with $AgNO_3$ solution. Afterwards, the solid was heated at 50 °C under vacuum to eliminate the residual solvent. The resulting solid is the silsesquioxane that contains the

1,4-diazoniabicyclo[2.2.2] octane nitrate group, which was applied as silver nanoparticles stabilizer.

Synthesis of silver nanoparticles (AgNP)

Aqueous solution (10.0 mL) containing 100 mg of ionic silsesquioxane, which contains the 1,4-diazoniabicyclo[2.2.2] octane nitrate group, was mixed with 1.0 mL of 3×10^{-3} mol L^{-1} $AgNO_3$. It was added to this mixture, 5 mL of 0.02 mol L^{-1} $NaBH_4$ freshly prepared, always under stirring. In these conditions, the concentration of silver is 2×10^{-5} g mL^{-1}. The silver nanoparticles stabilized by the ionic silsesquioxane were hereafter called as AgNP. For comparison a reference solution, without metal precursor addition, was also prepared and it was designated as blank.

Deposition of silver nanoparticles films onto glass slide surfaces (AgNP films)

The glass slides (2.6 × 7.6 cm) were pretreated by immersion into NaOH 1 mol L^{-1} for 3 h at 65 °C, followed by immersion into HCl 1 mol L^{-1} for 1 h, in ultrasound bath, at room temperature. After that, the glass slides were dried under a N_2 stream. The AgNP films were obtained onto pretreated glass substrates by using the dip-coating technique. The substrates were exposed to 20 dips in AgNP aqueous dispersion, with velocity of 2.7 mm s^{-1} and interval of 32 min between each dip. Afterwards, the glass slides were submitted to thermal treatment in air employing an oven at different temperatures: 80, 140, 170 and 200 °C for 1 h.

Characterization

X-ray diffraction

The measurement of the dried AgNP dispersion was carried out by Siemens diffractometer model D500 using CuKα as X-ray source (λ = 0.154056 nm) at a generator voltage of 40 kV and a generator current of 17.5 mA.

UV-Vis analysis

The spectrum of AgNP aqueous dispersion was carried out at room temperature using a UV-160 1PC Shimadzu spectrophotometer and distilled water was used as reference. For the solid samples (thin films), a double beam spectrophotometer Agilent CARY 5000 was used to perform measurements of the total light reflectance (%R) and transmittance (%T) using an integrate sphere accessory (wavelength range of 350-800 nm). The percentage of light absorbed (%Abs) by the AgNP films and blank was calculated using the expression:

$$\%Abs = 100 - \%T - \%R \quad (1)$$

The absorbance due to only silver nanoparticles was obtained by the following expression:

$$\%Abs\ \text{silver nanoparticles} = \%Abs\ (\text{AgNP film}) - \%Abs\ (\text{blank}) \quad (2)$$

Transmission electron microscopy

Images of AgNP dispersion and AgNP films were recorded using a JEOL JEM-1220 microscope, operated at an acceleration voltage of 80 kV. The samples were prepared by placing two drops of aqueous AgNP dispersion onto carbon-coated Cu grid, and for the films, it was placed two drops of AgNP film fragments dispersed in isopropanol onto a carbon-coated Cu grid, followed by drying at ambient conditions. The size distribution of the silver nanoparticles was determined using the Quantikov software.

Atomic force microscopy (AFM)

The surface morphology of films was obtained using an Agilent Technologies model 5500 SPM in acoustic mode. The used tips were of silicon (10 nm of diameter vertex) with a nominal spring constant of 40 N m^{-1}, resonance frequency of 142 kHz. The ratio between the amplitude of free oscillation and the amplitude maintained for one scan was kept constant near 50%, minimizing the effects of adhesion and maximizing the effects of viscoelasticity. To maximize the contribution of changes in the viscoelastic properties the signal (x) was detected at angle θ + 90°.[58] Images of 1 μm × 1 μm were obtained and analyzed by WSxM 6.0 software developed by Nanotec Electronic SL.

Spectral ellipsometry

Ellipsometry is a powerful technique to investigate optical properties of bulk materials and thin films.[53] The technique performs the analysis of the light polarization state after the interaction of light with the sample, usually in reflection, which is related to the optical properties of the material by the fundamental ellipsometry equation:

$$\frac{r_p}{r_s} = e^{-i\Delta} \tan(\psi) \quad (3)$$

where Δ and tan(ψ) are the phase shift and amplitude ratio, respectively, between the p and s polarization components of light. Particularly, in the case of thin films, r_p and r_s are the Drude reflection coefficients and are dependent of: the angle of incidence (θ) and wavelength (λ) of the light; film

thickness (d) and dispersion curves of air $N_0(\lambda)$; substrate $Ns(\lambda)$ and film $Nf(\lambda)$. These dispersion curves present the form $N(\lambda) = n_f(\lambda) + ik_f(\lambda)$, where $n_f(\lambda)$ and $k_f(\lambda)$ are, respectively, the real and imaginary parts of the refractive index. The measurements were performed using a spectral ellipsometer Sopra GES-5E (light wavelength range of 350 to 800 nm and incident angle of 68°) with a special accessory to measure thin films: a set of lenses to focus the incident light beam in a small area at the sample surface and then collecting only the light reflected from the film. The ellipsometer analysis software WinElli was used to determinate the thicknesses of the films through adjusting a dispersion curve model to the experimental data through the equation 3. The model used in this analysis will be discussed in details in the results and discussion section.

Thermogravimetric analysis

The thermal stability of films was performed under nitrogen flow on a TA Instrument system model TGA Q5000, with a heating rate of 10 °C min^{-1}, from room temperature up to 700 °C. In this analysis, several glass slides were scraped to obtain enough quantity of sample. It was used a blank sample (film without AgNP) for comparison.

Antibacterial activity

The antibacterial activity of the films was assessed against *Staphylococcus aureus* (*S. aureus*, ATCC 6538) using the FAC method (film applicator coating).[59] Firstly, the culture was grown in tryptic soy broth (TSB, Merck) at 37 ºC. After 16 h of incubation, *S. aureus* cells were washed with sterile saline solution (0.9 %) and diluted to reach an optical density (O.D. 600 nm) of 0.180 (ca. 108 colony forming units *per* mL, CFU mL^{-1}). Then, 50 µL of the diluted suspension were applied to the AgNP films and to the control sample (glass slide only). After that, the samples were kept at room temperature in wet boxes for 24 h. Then the bacterial suspensions were transferred separately into eppendorf tubes containing sterile saline solution in order to perform serial dilutions. Subsequently, cells of *S. aureus* (10 µL) from dilutions were spread evenly on tryptic soy agar (TSA, Merck), and the plates were incubated at 37 °C for 24 h. The viable *S. aureus* cells were estimated by counting bacterial colonies on the plates. The bactericidal effect was calculated as a percentage of inhibition, which was obtained by the following equation:

$$\text{Bactericidal ratio} = (\text{CFU of control} - \text{CFU of AgNp film}) / \text{CFU of control} \quad (4)$$

In order to evaluate the possibility of reusing the AgNP film, the samples were subjected three times to the experiments of antibacterial activity. Between every antibacterial activity test, the AgNP film and the control sample were cleaned with distilled water and sterilized by dry heating at 170 ºC, for 1 h.

Results and Discussion

The ionic silsesquioxane that contains the double charged 1,4-diazoniabicyclo[2.2.2]octane nitrate group was prepared and its structure is represented in Figure 1. Due to the presence of charged organic group this material shows appreciable solubility in water,[48,49,60] and also it presents the inorganic silica component. These characteristics allow the use of ionic silsesquioxanes as stabilizer of metal nanoparticles in aqueous medium.[47,50] In recent paper,[56] trying to elucidate the mechanism of metal nanoparticle stabilization by ionic silsesquioxane, it was made zeta potential measurements for this system. For ionic silsesquioxane, without silver nanoparticles, the zeta potential was +8.3 mV, and it was assigned to the presence of quaternary ammonium groups. For the nanoparticles stabilized by ionic silsesquioxane the zeta potential was +24.7 mV, indicating that the nanoparticles have positive charge on surface. Therefore, this charge is able to contribute for an electrostatic stabilization. It was reported that nanoparticles with zeta potential above +25 mV are considered to present highly charged surfaces, however, only above +40 mV they are considered just to be stabilized by electrostatic effects.[61,62] Therefore, the stabilization should present also a steric component, because the stabilizer is a polymer, a silica based hybrid material, which contains Si–O–Si linkages, as represented in the scheme of Figure 1.

Another interesting characteristic of the ionic silsesquioxane is the presence of polymerizable silanol groups (Figure 1). The silanol groups allow the silsesquioxane to attach covalently onto silica, alumina and glass surfaces.[53-55]

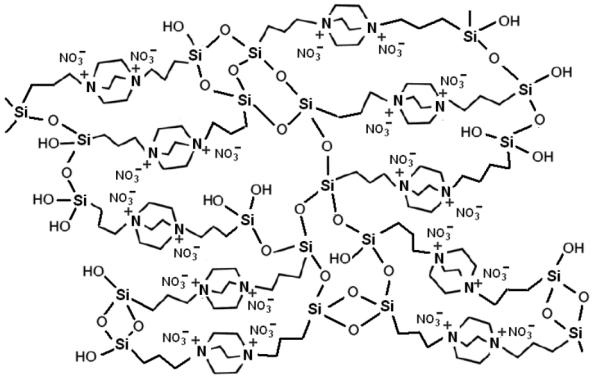

Figure 1. Representation of ionic silsesquioxane structure.

This strong affinity of ionic silsesquioxane with inorganic matrix surfaces was already reported for porous materials, and was ascribed to Si–O–Si bonds.[48] Therefore, considering both features, metal nanoparticles stabilization and ability to form coatings, films of silver nanoparticles were obtained on flat glass surfaces by dipping the glass slides in aqueous dispersion of silver nanoparticle stabilized by the ionic silsesquioxane (AgNP). The AgNP films present yellow color and transparency similar to the AgNP aqueous dispersion, which is typical of spherical and well-dispersed silver nanoparticles.[56,63] The AgNP films were heated at different temperatures in order to evaluate their thermal stability.

The UV-Vis spectra of the AgNP films with heat treatment at different temperatures, as well as for the AgNP aqueous dispersion, are presented in Figure 2. It is possible to observe a plasmon resonance absorption band with a maximum at 408 nm for the AgNP aqueous dispersion. However, a redshift was observed for the spectra of all AgNP films. The redshift of the maximum absorption band of the films in relation to the aqueous dispersion can be attributed to a higher proximity of silver nanoparticles in the films. The closeness of metal nanoparticles can result in a decrease in the plasmon resonance energy, producing shifts towards longer wavelengths in the spectrum.[64] However, it should be considered additional effects due to the matrix medium, such as density and refraction index, which modify the absorption maxima position, since the silver nanoparticles change from the aqueous dispersion to film medium. It is also possible to observe a second redshift effect with increasing thermal treatment temperature. The plasmon resonance band starts with a maximum at 427 nm for AgNP film at room temperature, shifting until 442 nm for AgNP film heat-treated up to 200 ºC. This trend can be assigned to the increasing size of the metal nanoparticles with the thermal treatment temperature, due to the coalescence mechanism.[33-36] This subject will be addressed afterwards. It is also observed that the heat treatment produces a decrease in the band intensity, mainly at 170 and 200 ºC. This trend could be interpreted as consequence of the interaction of metal nanoparticles with the glass substrate or also due to the formation of silver oxide, as reported elsewhere.[27,28,33]

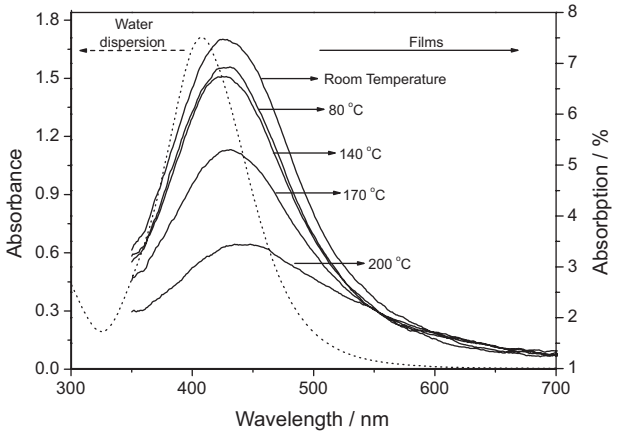

Figure 2. UV-Vis spectra of AgNP aqueous dispersion and AgNP films, heat treated at different temperatures.

TEM images of the AgNP films and the size distribution curves are presented in Figure 3. For all temperatures of treatment, it is possible to see silver nanoparticles close to one another, with spherical shape and uniformly dispersed in the films. The average size of metal nanoparticles in AgNP aqueous dispersion was 2.8 nm with a standard deviation of 1.3 nm. For the AgNP film without heating (room temperature) the average size of the nanoparticles was 2.4 nm with standard deviation of 0.7 nm. The average

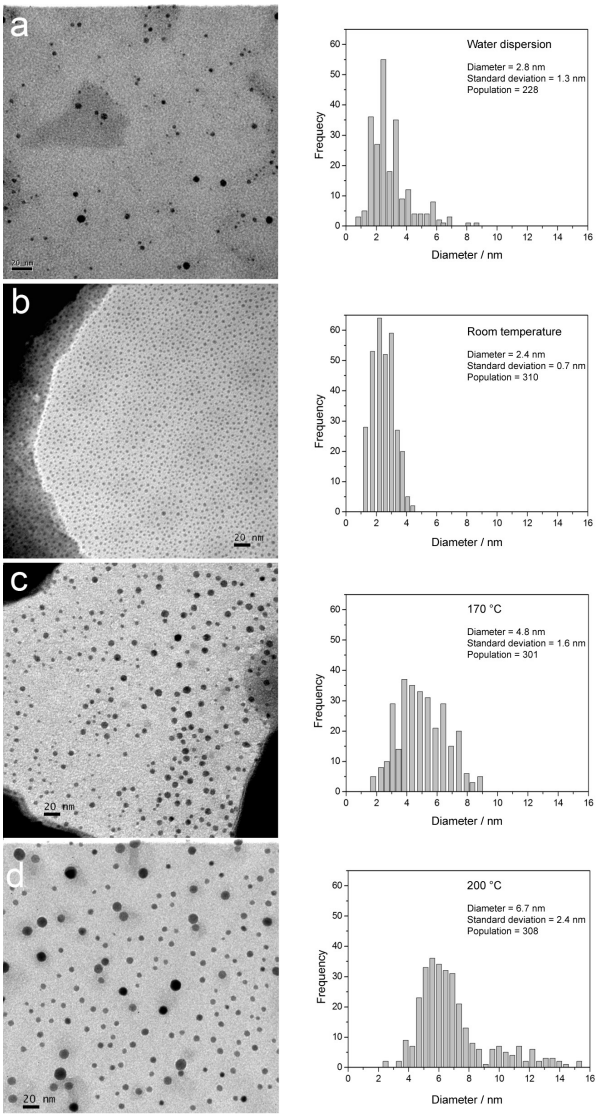

Figure 3. TEM images of AgNP and size distribution: (a) AgNP aqueous dispersion; (b) AgNP film at room temperature; (c) AgNP film heat treated at 170 ºC and (d) AgNP film heat treated at 200 ºC.

size of nanoparticles and the standard deviation for this film were little bit lower than those of the nanoparticles in aqueous dispersion. This small difference is clearly visible in the Figures 3a and 3b. This result shows that there was a selection process during the film formation, where the larger metal nanoparticles, with size above 5 nm were not incorporated in the film, resulting also in a small decrease in the standard deviation. However, the heat treatment at 170 ºC leads to an increasing in the silver nanoparticles size to 4.8 nm with standard deviation of 1.6 nm. Further thermal treatment up to 200 ºC results in larger average size, 6.7 nm, with standard deviation of 2.4 nm. This metal nanoparticle increase was interpreted by taking into account the coalescence process due to the metal nanoparticles closeness. It is important to point out that even after thermal treatment at 200 ºC, the size of silver nanoparticles remains below 10 nm, where absorption properties are dominant, which is a desirable characteristic for optical devices, enlarging the possibilities of applications.[23]

To evaluate the physical thickness of the AgNP films using ellipsometry, it was necessary to modeling correctly their dispersion curves. Thus, the films were considerate homogeneous and isotropic in the ellipsometer analysis software. However, due to the presence of silver nanoparticles, which presents a characteristic and localized absorption peak, the simple dispersion model of Cauchy[65] for dielectric and low absorption films was not sufficient to obtain a correct fitting to experimental data. It was necessary the use of an additional Drude-Lorentz term with the Cauchy model in the dispersion curves $n_f(\lambda)$ and $k_f(\lambda)$, which are related to the real ($\varepsilon_r(\lambda)$) and imaginary ($\varepsilon_i(\lambda)$) dielectric constants from the material, as follow:

$$n_f(\lambda) = \left[\frac{\left(\varepsilon_r^2(\lambda) + \varepsilon_i^2(\lambda)\right)^{\frac{1}{2}} + \varepsilon_r(\lambda)}{2} \right]^{\frac{1}{2}} \quad (5)$$

$$n_f(\lambda) = \left[\frac{\left(\varepsilon_r^2(\lambda) + \varepsilon_i^2(\lambda)\right)^{\frac{1}{2}} + \varepsilon_r(\lambda)}{2} \right]^{\frac{1}{2}} \quad (6)$$

where $\varepsilon_r(\lambda) = \varepsilon_r^C(\lambda) + \varepsilon_r^L(\lambda)$ and $\varepsilon_i(\lambda) = \varepsilon_i^C(\lambda) + \varepsilon_i^L(\lambda)$.

The C and L indices in the terms above indicate the Cauchy and Drude-Lorentz contributions to dielectric constants that are defined as:

$$\varepsilon_r^c(\lambda) = \left(A + \frac{B}{\lambda^2} + \frac{C}{\lambda^4} \right)^2 + \left(\frac{D}{\lambda} + \frac{E}{\lambda^3} + \frac{F}{\lambda^5} \right)^2 \quad (7)$$

$$\varepsilon_i^c(\lambda) = 2\left(A + \frac{B}{\lambda^2} + \frac{C}{\lambda^4} \right)\left(\frac{D}{\lambda} + \frac{E}{\lambda^3} + \frac{F}{\lambda^5} \right) \quad (8)$$

$$\varepsilon_r^L(\lambda) = \frac{A_0 \lambda^2 \left(\lambda^2 - E_o^2\right)}{\left(\lambda^2 - E_o^2\right)^2 + \gamma^2 \lambda^2} \quad (9)$$

$$\varepsilon_i^L(\lambda) = \frac{A_0 \lambda^3 \gamma}{\left(\lambda^2 - E_o^2\right)^2 + \gamma^2 \lambda^2} \quad (10)$$

where A, B, C, D, E and F are constants, A_0, E_o and γ are, respectively, the amplitude, the central wavelength and width of Lorentz absorption peak.

Using the model above, it was possible to fit it to the experimental data with a $R^2 > 0.977$ for all films ($R^2 = 1$ means a perfect fitting) and to obtain respective film physical thicknesses, as presented in Figure 4. As can be seen in this Figure, the film thickness presents a stable value (around 45 nm) during the entirely heat treatment, even after heated up to 200 ºC.

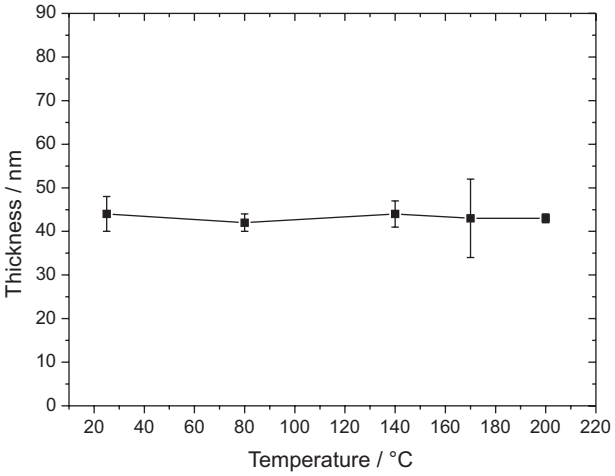

Figure 4. Evolution of film thickness with the heat treatment.

The phase contrast images obtained by AFM for AgNP films at room temperature and heated to 200 ºC are shown in Figure 5 together with blank samples. It is possible to observe the existence of bright contrast with darker regions in the images, which are derived from the difference in hardness between the materials contained in the film surface. The lighter regions are related to the presence of a softer material than the dark region.[58] For AgNP film images, dark spots were observed, which can be assigned to the silver nanoparticles. The thermal treatment did not produce significant changes on blank films. On the other hand, in the AgNP films an increasing in the darker spots size was observed after thermal treatment at 200 ºC, in agreement to the TEM images. Additionally, the phase contrast images show that the silver nanoparticles are near to the film surface, and this characteristic is desirable for this material, since the nanoparticles need a direct

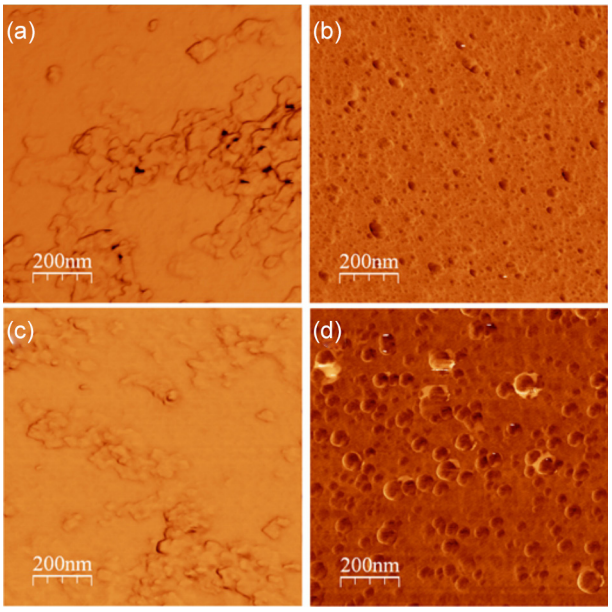

Figure 5. Phase contrast images obtained by AFM. (a) Blank film at room temperature; (b) AgNP film at room temperature; (c) blank film heated to 200 ºC; (d) AgNP film heated to 200 ºC.

contact with the bacteria to ensure good performance as antibacterial material.

Topography images of AgNP films, obtained by AFM, are presented in Figure 6. It is possible to observe that the AgNP film heated to 200 ºC presents roughness higher than the not heat treated AgNP film. The roughness was estimated by RMS (root mean square) using WSxM software. The values found were 10 nm for room temperature AgNP film and 20 nm for AgNP film heat treated to 200 ºC. However, it is important to emphasize that the roughness measurements were obtained in localized points of the film surface, and these results are not in disagreement to the ellipsometry technique, which reflects the thickness of whole film.

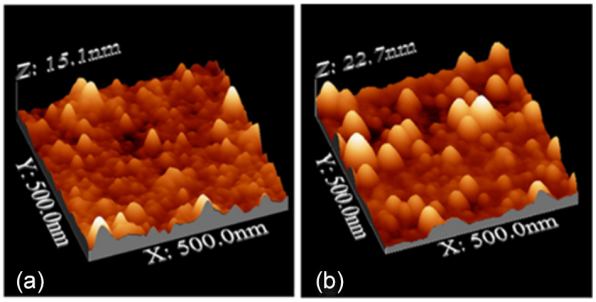

Figure 6. Topography image of AgNP film: (a) at room temperature; (b) at 200 °C.

Figure 7 shows TGA curves of blank and AgNP films. Both curves show two main weight losses, the first occurs up to 100 °C due to the water desorption and the second one appears in the temperature range between 220-350 °C,

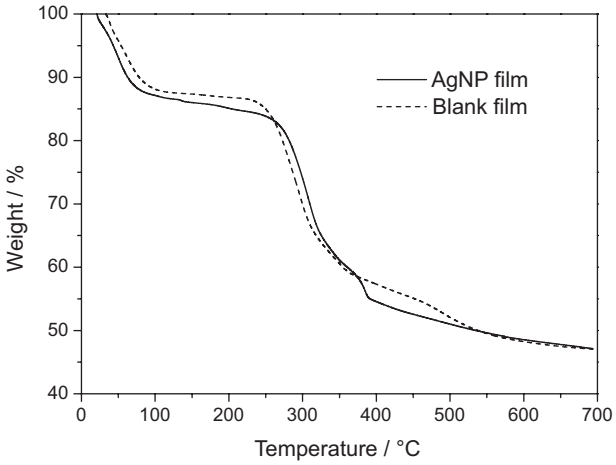

Figure 7. TGA curves of blank and AgNP films.

which was assigned to the decomposition of the organic moiety of the silsesquioxane.[66] These results confirm the thermal stability of the AgNP film, at least, after thermal treatment up to 200 ºC, in accordance to TEM, UV-Vis, AFM and ellipsometry analysis presented above. Therefore, this material presents the necessary characteristics to be used in systems that require sterilization like food package or hospital instruments.

Considering that the AgNP aqueous dispersion showed excellent antibacterial activity against *S. aureus* allied to low cytotoxicity,[56] it was evaluated the possibility of using the AgNP films as bactericidal coatings, the films were tested against *S. aureus*, which is a very common bacterium responsible for hospital infections. On the Table 1, it is shown the bactericidal activity of the AgNP film at room temperature, followed by dry sterilization cycles at 170 ºC for 1 h. It is possible to observe that the blank film presents bactericidal activity similar to that of the AgNP film, before the sterilization cycles. This activity was assigned to the quaternary ammonium groups of the ionic silsesquioxane. However, the sterilization process leads to a drastic decrease in this activity after the second sterilization cycle. This decrease can be ascribed to a partial decomposition of the ammonium groups due to the continuous heat treatment for 1 h. Simultaneously

Table 1. Bactericidal activity of AgNP and blank films against *S. aureus* bacterium, before and after the dry sterilization process at 170 ºC, for 1 h

Cycle	Bactericidal activity / %[a]	
	AgNP film	Blank film
Without sterilization	100	100
After sterilization 1	99	78
After sterilization 2	98	0
After sterilization 3	99	0

[a]Error lower than 5 %.

occurred the network crosslinking forming siloxane bonds, which maintain the bulk and the thickness of the film. On the other hand, the AgNP film presents an excellent performance even after the third cycle of sterilization, showing that the silver nanoparticles maintain their bactericidal properties.

The Figure 8 illustrates the bacterium growing for one sample of the series after the sterilization 1, using the FAC method, which was appropriate for this estimation in the present case.

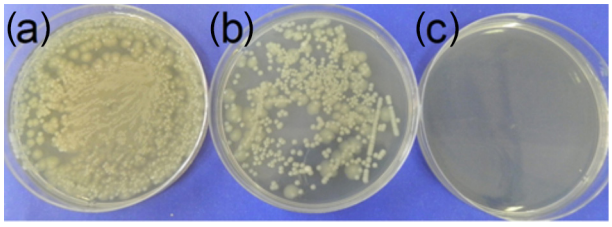

Figure 8. *S. aureus* bacterium growing in the presence of: (a) control samples; (b) blank film and; (c) AgNP film room temperature.

Conclusions

Thin films containing silver nanoparticles with diameter lower than 10 nm were deposited on flat glass substrate. The films were prepared by using an ionic silsesquioxane as metal nanoparticles stabilizer and crosslinking agent. The films were thermally stable up to 200 ºC, keeping their weight and thickness near to 45 nm for all temperatures of treatment. From UV-Vis and TEM, it was observed that the silver nanoparticles are very close to one another, with spherical shape and uniformly dispersed in the films. They present an increase in the size with the increasing temperature treatment, from 2.4 nm at room temperature to 6.7 nm at 200 ºC. The AFM confirmed the metal nanoparticle size increase with the temperature elevation, and showed that they are on the surface of the film. The films showed an excellent activity against *S. aureus* bacterium, even after three sterilization cycles at 170 ºC, making them promising to be applied in systems that require sterilization.

Acknowledgements

The authors are grateful to CNPQ (Conselho Nacional de Desenvolvimento Científico e Tecnológico), FAPERGS (Fundação de Amparo à Pesquisa do Estado do Rio Grande do Sul) and CAPES (Coordenação de Aperfeiçoamento Pessoal de Nível Superior) for financial support and the fellowship awards. We also thank the Centro de Microscopia Eletrônica da Universidade Federal do Rio Grande do Sul for TEM images.

References

1. Angelomé, P. C.; Liz-Marzán, L. M.; *J. Sol-Gel Sci. Technol.* **2014**, *70*, 180.
2. Nilius, N.; Risse, T.; Schauermann, S.; Shaikhutdinov, S.; Sterrer, M.; Freund, H.-J.; *Top. Catal.* **2011**, *54*, 4.
3. Hariprasad, E.; Radhakrishnan, T. P.; *ACS Catal*. **2012**, *2*, 1179.
4. Dinda, E.; Rashid, M. H.; Biswas, M.; Mandal, T. K.; *Langmuir* **2010**, *26*, 17568.
5. Akgun, B. A.; Wren, A. W.; Durucan, C.; Towler, M. R.; Mellott, N. P.; *J. Sol-Gel Sci. Technol.* **2011**, *59*, 228.
6. Akhavan, O.; Ghaderi, E.; *Curr. Appl. Phys.* **2009**, *9*, 1381.
7. Fu, Y.; Li, G.; Tian, M.; Wang, X.; Zhang, L.; Wang, W.; *J. Appl. Polymer Sci.* **2014**, *131*, 39859.
8. Ivanova, E. P.; Hasan, J.; Truong, V. K.; Wang, J. Y.; Raveggi, M.; Fluke, C.; Crawford, R. J.; *Appl. Microbiol. Biotechnol.* **2011**, *91*, 1149.
9. Juan, L.; Zhimin, Z.; Anchun, M.; Lei, L.; Jingchao, Z.; *Int. J. Nanomed*. **2010**, *5*, 261.
10. Wang, Q.; Yu, H.; Zhong, L.; Liu, J.; Sun, J.; Shen, J.; *Chem. Mater.* **2006**, *18*, 1988.
11. de Faria, A. F.; Martinez, D. S.; Meira, S. M. M.; de Moraes, A. C. M.; Brandelli, A.; Filho, A. G. S.; Alves, O. L.; *Colloid Surf. B* **2014**, *113*, 115.
12. da Silva, A. L. C. M.; Gutierres, M. G.; Thesing, A.; Lattuada, R. M.; Ferreira, J.; *J. Braz. Chem. Soc.* **2014**, *25*, 928.
13. Lee, Y.; Koh, K.; Na, H.; Kim, K.; Kang, J.-J.; Kim, J.; *Nanoscale Res. Lett*. **2009**, *4*, 364.
14. Ye, J.; Bonroy, K.; Nelis, D.; Frederix, F.; D'Haen, J.; Maes, G.; Borghs, G.; *Colloid Surf. A* **2008**, *321*, 313.
15. Brandon, M. P.; Ledwith, D. M.; Kelly, J. M.; *J. Colloid Interface Sci.* **2014**, *415*, 77.
16. Guiet, A.; Reier, T.; Heidary, N.; Felkel, D.; Johnson, B.; Vainio, U.; Schlaad, H.; Aksu, Y.; Driess, M.; Strasser, P.; Thomas, A.; Polte, J.; Fischer, A.; *Chem. Mater.* **2013**, *25*, 4645.
17. Gooding, J. J.; Alam, M. T.; Barfidokht, A.; Carter, L.; *J. Braz. Chem. Soc.* **2014**, *25*, 418.
18. Kozlovskaya, V.; Kharlampieva, E.; Khanal, B. P.; Manna, P.; Zubarev, E. R.; Tsukruk, V. V.; *Chem. Mater.* **2008**, *20*, 7474.
19. Kulkarni, A. P.; Noone, K. M.; Munechika, K.; Guyer, S. R.; Ginger, D. S.; *Nano Lett.* **2010**, *10*, 1501.
20. Mubeen, S.; Hernandez-Sosa, G.; Moses, D.; Lee, J.; Moskovits, M.; *Nano Lett.* **2011**, *11*, 5548.
21. Wu, J.-L.; Chen, F. C.; Hsiao, Y.-S.; Chien, F.-C.; Chen, P.; Kuo, C.-H.; Huang, M. H.; Hsu, C.-S.; *ACS Nano* **2011**, *5*, 959.
22. Willets, K.; van Duyne, R. P.; *Annu. Rev. Phys. Chem.* **2007**, *58*, 267.
23. Akjouj, A.; Lévêque, G.; Szunerits, S.; Pennec, Y.; Djafari-Rouhani, B.; Boukherroub, R.; Dobrzynski, L.; *Surf. Sci. Rep.* **2013**, *68*, 1.

24. Aiken, J. D.; Finke, R. G.; *J. Mol. Catal. A* **1999**, *145*, 1.
25. Bernardo-Gavito, R.; Serrano, A.; García, M. A.; Miranda, R.; Granados, D.; *J. Appl. Phys.* **2013**, *114*, 164312.
26. Lu, J.-L.; Weissenrieder, J.; Kaya, S.; Gao, H.-J.; Shaikhutdinov, S.; Freund, H.-J.; *Surf. Rev. Lett.* **2007**, *14*, 927.
27. Babapour, A.; Akhavan, O.; Azimirad, R.; Moshfegh, A. Z.; *Nanotechnology* **2006**, *17*, 763.
28. Li, W.; Seal, S.; Megan, E.; Ramsdell, J.; Scammon, K.; Legon, G.; Lachal, L.; Richardson, K. A.; *J. Appl. Phys.* **2003**, *93*, 9553.
29. Yliniemi, K.; Ebbinghaus, P.; Keil, P.; Kontturi, K.; Grundmeier, G.; *Surf. Coat. Technol.* **2007**, *201*, 7865.
30. Yliniemi, K.; Vahvaselka, M.; van Ingelgem, Y.; Baert, K.; Wilson, B. P.; Terryn, H.; Kontturi, K.; *J. Mater. Chem. B* **2008**, *18*, 199.
31. Gaspera, E. D.; Karg, M.; Baldauf, J.; Jasieniak, J.; Maggioni, G.; Martucci, A.; *Langmuir* **2011**, *27*, 13739.
32. Grabar, K. C.; Freeman, R. G.; Hommer, M. B.; Natan, M. J.; *Anal. Chem.* **1995**, *67*, 735.
33. Karakouz, T.; Maoz, B. M.; Lando, G.; Vaskevich, A.; Rubinstein, I.; *ACS Appl. Mater. Interfaces* **2011**, *3*, 978.
34. Bhatta, U. M.; Khushalani, D.; Satyam, P. V.; *Bull. Mater. Sci.* **2011**, *34*, 595.
35. Supriya, L.; Claus, R. O.; *Chem. Mater.* **2005**, *17*, 4325.
36. Volkman, S. K.; Yin, S.; Bakhishev, T.; Puntambekar, K.; Subramanian, V.; Toney, M. F.; *Chem. Mater.* **2011**, *23*, 4634.
37. Bonnemann, H.; Richards, R. M.; *Eur. J. Inorg. Chem.* **2001**, *2001*, 2455.
38. Tsuji, M.; Ogino, M.; Matsuo, R.; Kumagae, H.; Hikino, S.; Kim, T.; Yoon, S.-H.; *Cryst. Growth Des.* **2010**, *10*, 296.
39. Gopidas, K. R.; Whitesell, J. K.; Fox, M. A.; Carolina, N.; *Nano Lett.* **2003**, *3*, 1757.
40. Pal, S.; Tak, Y. K.; Song, J. M.; *Appl. Environm. Microbiol.* **2007**, *73*, 1712.
41. Duncan, T. V.; *J. Colloid Interface Sci.* **2011**, *363*, 1.
42. Silva, J. M. S.; Pastorello, M.; Kobarg, J.; Cardoso, M. B.; Mazali, I. O.; *ChemPhysChem.* **2013**, *14*, 4075.
43. Chaloupka, K.; Malam, Y.; Seifalian, A. M.; *Trends Biotechnol.* **2010**, *28*, 580.
44. Marambio-Jones, C.; Hoek, E. M. V.; *J. Nanopart. Res.* **2010**, *12*, 1531.
45. Siegel, J.; Polívková, M.; Kasálková, N. S.; Kolská, Z.; Svorcik, V.; *Nanoscale Res. Lett.* **2013**, *8*, 388.
46. Marcato, P. D.; Parizotto, N. V.; Martinez, D. S. T.; Paula, A. J.; Ferreira, I. R.; Melo, P. S.; Durán, N.; Alves, O. L.; *J. Braz. Chem. Soc*. **2013**, *24*, 266.
47. Nunes, M. R.; Gushikem, Y.; Landers, R.; Dupont, J.; Costa, T. M. H.; Benvenutti, E. V.; *J. Sol-Gel Sci. Technol.* **2012**, *63*, 258.
48. Arenas, L. T.; Langaro, A.; Gushikem, Y.; Moro, C. C.; Benvenutti, E. V.; Costa, T. M. H.; *J. Sol-Gel Sci. Technol*. **2003**, *28*, 51.
49. Gushikem, Y.; Benvenutti, E. V.; Kholin, Y. V.; *Pure Appl. Chem.* **2008**, *80*, 1593.
50. de Menezes, E. W.; Nunes, M. R.; Arenas, L. T.; Dias, S. L. P.; Garcia, I. T. S.; Gushikem, Y.; Costa, T. M. H.; Benvenutti, E. V.; *J. Solid State Electrochem.* **2012**, *16*, 3703.
51. Arenas, L. T.; Aguirre, T. A. S.; Langaro, A.; Gushikem, Y.; Benvenutti, E. V.; Costa, T. M. H.; *Polymer* **2003**, *44*, 5521.
52. de Menezes, E. W.; Lima, E. C.; Royer, B.; de Souza, F. E.; dos Santos, B. D.; Gregório, J. R.; Costa, T. M. H.; Gushikem, Y.; Benvenutti, E. V.; *J. Colloid Interface Sci.* **2012**, *378*, 10.
53. Pereira, M. B.; Michels, A. F.; Gay, D. S. F.; Benvenutti, E. V.; Costa, T. M. H.; Horowitz, F.; *Opt. Mater.* **2010**, *32*, 1170.
54. Gay, D. S. F.; Fernandes, T. H. M.; Amavisca, C. V.; Cardoso, N. F.; Benvenutti, E. V.; Costa, T. M. H.; Lima, E. C.; *Desalination* **2010**, *258*, 128.
55. Caldas, E. M.; de Menezes, E. W.; Pizzolato, T. M.; Dias, S. L. P.; Costa, T. M. H.; Arenas, L. T.; Benvenutti, E. V.; *J. Sol-Gel Sci. Technol.* **2014**, *72*, 282.
56. Schneid, A. C.; Roesch, E. W.; Sperb, F.; Matte, U.; da Silveira, N. P.; Costa, T. M. H.; Benvenutti, E. V.; de Menezes, E. W.; *J. Mater. Chem. B* **2014**, *2*, 1079.
57. Arenas, L. T.; Dias, S. L. P.; Moro, C. C.; Costa, T. M. H.; Benvenutti, E. V.; Lucho, A. M. S.; Gushikem, Y.; *J. Colloid Interface Sci.* **2006**, *297*, 244.
58. Ragha, D.; van Landingham, M.; Gu, X.; Nguyen, T.; *Langmuir* **2000**, *16*, 9448.
59. Juan, L.; Zhimin, Z.; Anchun, M.; Lei, L.; Jingchao, Z.; *Int. J. Nanomed.* **2010**, *5*, 261.
60. da Trindade, C. M.; Stoll, G. C.; Pereira, A. S.; Costa, T. M. H.; Benvenutti, E. V.; *J. Braz. Chem. Soc.* **2009**, *20*, 737.
61. Yu, W.; Xie, H.; *J. Nanomater.* **2012**, *2012*, 435873.
62. Tanvir, S.; Oudet, F.; Pulvina S.; Anderson, W. A.; *Enzyme Microb. Technol*. **2012**, *51*, 231.
63. Wei, D.; Sun, W.; Qian, W.; Ye, Y.; Ma, X.; *Carbohydr. Res.* **2009**, *344*, 2375.
64. Jensen, T. R.; Malinsky, M. D.; Haynes, C. L.; van Duyne, R. P.; *J. Phys. Chem. B* **2000**, *104*, 10549.
65. Soave, P. A.; Dau, R. A. F.; Becker, M. R.; Pereira, M. B.; Horowitz, F.; *Opt. Engineer.* **2009**, *48*, 124603.
66. Arenas, L. T.; Pinheiro, A. C.; Ferreira, J. D.; Livotto, P. R.; Pereira, V. P.; Gallas, M. R.; Gushikem, Y.; Costa, T. M. H.; Benvenutti, E. V.; *J. Colloid Interface Sci.* **2008**, *318*, 96.

Submitted: September 30, 2014
Published online: March 20, 2015

FAPERGS has sponsored the publication of this article.